Chem. Mater. **2007,** *19,* 6597–6604

Structural and Magnetic Properties of Cobalt Nanoparticles Encased in Siliceous Shells

Michael A. Zalich,[†,§] Michael L. Vadala,[§] Judy S. Riffle,[§] Martin Saunders,[‡] and Timothy G. St. Pierre*[,†]

School of Physics and Center for Microscopy and Microanalysis, The University of Western Australia, 35 Stirling Highway, Crawley WA 6009, Australia, and Department of Chemistry and Macromolecules and Interfaces Institute, Virginia Polytechnic Institute and State University, Blacksburg, Virginia 24061

Received February 23, 2006. Revised Manuscript Received June 12, 2007

Stable colloidal dispersions of cobalt nanoparticles were prepared by refluxing toluene solutions of dicobalt octacarbonyl in the presence of poly(dimethylsiloxane-*b*-(methylvinylsiloxane-*co*-methyl(2-trimethoxysilethyl)siloxane)) (PDMS-*b*-(PMVS-*co*-PMTMS)) dispersion stabilizers. The nanoparticles coated with the polysiloxane copolymer were subsequently heated at 600 or 700 °C with the goal of forming siliceous shells on the cobalt surfaces to protect them from oxidation. The thermolysis processes at 600 and 700 °C produced increases in the cobalt specific saturation magnetizations (σ_s) from 48 to 141 and 146 emu g^{-1} of cobalt respectively. The siliceous coatings provided oxidative protection under ambient conditions for long periods. However, mechanically grinding the thermally treated nanoparticles led to decreases in σ_s upon aging in air. Particle size analyses indicated an increase in average particle size in the materials heated at 600 °C, but the materials that were heated at 700 °C retained their small nanoparticle sizes. Electron diffraction and X-ray diffraction confirmed that the heat-treated cobalt nanoparticles were predominantly in the face-centered cubic phase, while the materials that had not been heated at the elevated temperatures were only weakly crystalline. Hence, the increases in σ_s from the preheat-treated to the heat-treated materials were attributed to an improvement in particle crystallinity, combined with less oxidation due to partial protection by a siliceous shell.

Introduction

One of the most exciting and rapidly growing areas of interest for magnetic nanoparticles is biomedicine. A number of current and potential applications for magnetic nanoparticles in medicine exist, ranging from MRI contrast enhancement agents[1] to tumor hyperthermia treatment.[2,3] Magnetite (Fe_3O_4) is of particular interest because of its biocompatibility. However, the saturation magnetization of magnetite (~90 emu g^{-1}) compared to Fe^0 (218 emu g^{-1}) or Co^0 (161 emu g^{-1}) may not be sufficient for some applications.

It would be advantageous to protect zero-valence cobalt nanoparticles against oxidation by passivating the particles with a protective coating, thereby enabling their usage in biotechnology. Relatively little is known regarding cobalt toxicity, but it is reasoned that a siliceous coating may protect against toxicity. Rutnakornpituk et al. and Stevenson et al. investigated the use of a polysiloxane triblock copolymer (poly(dimethylsiloxane-*b*-(3-cyanopropyl)methylsiloxane-*b*-dimethylsiloxane); PDMS-PCPMS-PDMS) in which the cyano groups were bound to the cobalt nanoparticles and the PDMS endblocks sterically stabilized the particles in organic solutions. The cobalt specific magnetization was reported to decrease over time,which was attributed to cobalt oxide formation.[4,5] Connolly et al. evaluated the magnetic properties of cobalt nanoparticles stabilized by a pentablock copolymer (poly(dimethylsiloxane-*b*-methyltriethoxysilethylsiloxane-*b*-(3-cyanopropyl)methylsiloxane-*b*-methyltriethoxysilethylsiloxane-*b*-dimethylsiloxane); PDMS-PMTEOS-PCPMS-PMTEOS-PDMS), where the cyano groups of the central block were bound to the cobalt nanoparticles, the PMTEOS blocks were condensed to form siliceous shells around the cobalt nanoparticles, and the PDMS blocks again sterically stabilized the nanoparticles in dispersions.[6] These cobalt−polymer complexes displayed improved oxidative stability, but the specific saturation magnetizations were relatively low. Vadala et al. recently reported the synthesis of a simpler polysiloxane

---

* Corresponding author. Phone: 61 8 6488 2747. Fax: 61 8 6488 1879. E-mail: stpierre@physics.uwa.edu.au.

[†] School of Physics, The University of Western Australia.

[‡] Center for Microscopy and Microanalysis, The University of Western Australia.

[§] Virginia Polytechnic Institute and State University.

(1) Boal, A. K., Synthesis and Application of Magnetic Nanoparticles. In *Nanoparticles: Building Blocks for Nanotechnology*, Rotello, V., Ed.; Kluwer Academic/Plenum Publishers: New York, 2004.

(2) Giri, J.; Pradhan, P.; Tvagi, N.; Banerjee, R.; Datta, D.; Bahadur, D. Synthesis, Characterization and In vitro Evaluation of Water-Based Temperature Sensitive Ferrofluids for Hyperthermia Applications. *Proceedings of the 5th International Conference on the Scientific and Clinical Applications of Magnetic Carriers*, Lyon, France, May 20−22, 2004; Hafeli, U., Ed.; The Cleveland Clinic Foundation: Cleveland, OH, 2004.

(3) Hilger, I.; Andra, W.; Hergt, R.; Hiergeist, R.; Kaiser, W. A. Treatment of Breast Cancer by Magnetic Heating. *Proceedings of the Fifth International Conference on the Scientific and Clinical Application of Magnetic Carriers*, Lyon, France, May 20−22, 2004; Hafeli, U., Ed; The Cleveland Clinic Foundation: Cleveland, OH, 2004.

(4) Rutnakornpituk, M.; Thompson, M. S.; Harris, L. A.; Farmer, K. E.; Esker, A. R.; Riffle, J. S.; Connolly, J.; St. Pierre, T. G. *Polymer* **2002**, *43*, 2337.

(5) Stevenson, J. P.; Riffle, J. S. *J. Magn. Magn. Mater.* **2001**, *225*, 47.

(6) Connolly, J.; St. Pierre, T. G.; Rutnakornpituk, M.; Riffle, J. S. *J. Phys. D: Appl. Phys.* **2004**, *37*, 2475.

10.1021/cm060458l CCC: $37.00

block copolymer, poly(dimethylsiloxane-*b*-(methylvinylsiloxane-*co*-methyl(2-trimethoxysilethyl)siloxane)); PDMS-*b*-(PMVS-*co*-PMTMS)), and methods to bind it to cobalt nanoparticles.[7] The pendent trialkoxysilyl groups on the second block bind to the cobalt, whereas the PDMS block stabilizes dispersions of these nanoparticles in toluene. These complexes were treated at elevated temperatures in an inert atmosphere in efforts to collapse protective siliceous shells around the nanoparticles. It is clear that the heat treatments also significantly improve the specific saturation magnetization. This paper describes the structural and magnetic properties of the cobalt-[PDMS-*b*-(PMVS-*co*-PMTMS)] nanoparticle assemblies, before and after heat treatments at 600 and 700 °C. The structural and magnetic properties were elucidated using transmission electron microscopy, X-ray photoelectron spectroscopy, electron diffraction, X-ray diffraction, small-angle X-ray scattering, and magnetic susceptometry.

Experimental Section

Materials. Hexamethylcyclotrisiloxane (D_3, Gelest, Inc.) was purified by stirring it over calcium hydride at 80 °C overnight and fractionally vacuum-distilling it under nitrogen into a preweighed, flame-dried flask. The *n*-butyllithium initiator was kindly donated by the Lithco Division of the FMC Corporation and was approximately 2.45 M in cyclohexane. It was titrated with diphenylacetic acid in THF until a yellow color persisted, and was used as received. 1,3,5-Trivinyl-1,3,5-trimethylcyclotrisiloxane (D_3^v, Gelest, Inc.) was fractionally distilled under vacuum into a predried flask, purged with nitrogen, sealed with a septum, and stored in a desiccator. Cyclohexane (Aldrich, 99%) was stirred with concentrated sulfuric acid for 48 h, washed with water, dried over $MgSO_4$ and then over sodium, and distilled just prior to use. Tetrahydrofuran (THF, 99.5%, E.M. Sciences) was dried over calcium hydride overnight and then refluxed over sodium in the presence of benzophenone until the solution was a deep purple. The THF was distilled just prior to use. Trimethylchlorosilane (Gelest, Inc.) was used as the terminating reagent for the diblock copolymers and was distilled before use. A Pt^0(1,3-divinyl-1,1,3,3-tetramethyldisiloxane)$_{1.5}$ complex catalyst in xylene (2.1–2.4 wt % Pt^0, Karstedt's catalyst; Gelest, Inc.) was used as received. Trimethoxysilane (Gelest, Inc.) was used as received. Toluene was washed twice with concentrated sulfuric acid and neutralized with water. It was dried over $MgSO_4$ for 1 h and then over calcium hydride overnight, and distilled just before use. $Co_2(CO)_8$ (Alpha Aesar) stabilized with 1–5% hexane was stored under argon in the freezer without further purification.

Table 1 describes the sample designations for the materials discussed in this paper. The composition and method of treatment and/or aging times for each sample are further described throughout the paper.

Synthesis of Poly(dimethylsiloxane-*b*-[methylvinylsiloxane-*co*-methyl-2-trimethoxysilethyl siloxane]) (PDMS-*b*-[PMVS-*co*-PMTMS]). A detailed synthetic procedure for PDMS-*b*-[PMVS-*co*-PMTMS] and the characterization of the precursors and final polymers have been reported recently.[7] Briefly, poly(dimethylsiloxane-*b*-methylvinylsiloxane) (PDMS-*b*-PMVS) was synthesized by the sequential polymerization of hexamethylcyclotrisiloxane (D_3) and 1,3,5-trivinyl-1,3,5-trimethylcyclotrisiloxane (D_3^v) monomers, initiated with *n*-butyllithium. Approximately half of the vinyl groups on the PMVS block were hydrosilated with trimethoxysilane to afford PDMS-*b*-[PMVS-*co*-PMTMS] block copolymers. The block copolymer used in this investigation had block lengths of 5000 and 3400 g mol^{-1} for the PDMS and PMVS-*co*-PMTMS blocks, respectively (Figure 1).

Table 1. Summary of Material Designations

material designations	coated cobalt complex
$\mathbf{N_1}$	complex without a high temperature heat treatment that was stored under N_2 or Ar
$\mathbf{N_{1a}}$ and $\mathbf{N_{1b}}$	complex without a high temperature heat treatment that was exposed to air: "a" was analyzed after 4 months, and "b" was analyzed after 15 months
$\mathbf{P_1}$	complex that was heated at 600 °C for 2 h and then exposed to air (not mechanically ground)
$\mathbf{P_{1a}}$ and $\mathbf{P_{1b}}$	complex that was heated at 600 °C for 2 h, mechanically ground, and then exposed to air; sample "a" was analyzed immediately after grinding, and sample "b" was analyzed after exposure for various times
$\mathbf{P_{2a}}$ and $\mathbf{P_{2b}}$	complex that was heated at 700 °C for 2 h, mechanically ground, and then exposed to air; sample "a" was analyzed immediately after grinding, and sample "b" was analyzed after exposure for various times

Synthesis of Cobalt Nanoparticles. Cobalt nanoparticles were synthesized by adding 1 g of dicobalt octacarbonyl into a reaction vessel containing 1 g of PDMS-*b*-[PMVS-*co*-PMTMS] dissolved in 20 mL of deoxygenated toluene. The reaction was refluxed at 110 °C for 2 h or until the disappearance of the $Co_4(CO)_{12}$ intermediate was observed with FTIR. After cooling, a stable magnetic dispersion of cobalt nanoparticles resulted. Toluene was removed under a vacuum to provide a dried sample for further experiments (referred to as $\mathbf{N_1}$). The material denoted as $\mathbf{N_1}$ was stored under argon or nitrogen at all times. Samples of this material were exposed to ambient air to evaluate the oxidative stability of the cobalt nanoparticles. The material designated $\mathbf{N_{1a}}$ was analyzed after exposure to ambient conditions for 4 months, and $\mathbf{N_{1b}}$ was analyzed after 15 months.

Heat Treatments of PDMS-*b*-[PMVS-*co*-PMTMS] Coated Cobalt Nanoparticles. A sample of $\mathbf{N_1}$ was transferred (with limited exposure to air) to a ceramic boat and inserted into a quartz tube furnace. It was held at 600 °C for 2 h (referred to as $\mathbf{P_{1a}}$) under a flow of argon. Another sample of $\mathbf{N_1}$ was heated at 700 °C for 2 h (referred to as $\mathbf{P_{2a}}$) under the same conditions. After the elevated heating processes, the samples were removed from the tube furnace and placed in separate vials under argon. The heat-treated materials were mechanically ground and exposed to ambient conditions for various periods, whereupon magnetic susceptometry measurements were conducted. The magnetic susceptometry measurements were conducted on $\mathbf{P_{1a}}$ and $\mathbf{P_{2a}}$ immediately after grinding. After grinding, $\mathbf{P_{1a}}$ and $\mathbf{P_{2a}}$ were aged (aged samples are designated $\mathbf{P_{1b}}$ and $\mathbf{P_{2b}}$) under ambient conditions for 6 months (180 days).

Transmission Electron Microscopy (TEM). TEM, high-resolution TEM, energy-filtered TEM, selected area electron diffraction (SAD), and nanobeam electron diffraction (NBD) were conducted with a JEOL 3000F field-emission transmission electron microscope (operated at 300 kV) equipped with a Gatan image filter (GIF) and digital imaging system. $\mathbf{N_{1a}}$, $\mathbf{P_{1a}}$, and $\mathbf{P_{2a}}$ were embedded in resin and microtomed to afford 50–100 nm thick slices. Microtomed slices were placed on amorphous carbon-coated copper grids for analysis. NBD was conducted on single crystals of $\mathbf{P_{1a}}$ with an ~2 nm focused electron beam. Particle size analyses were performed on two fields of view for each sample. Each field of view was divided into sections and all of the particles in a particular section were measured in two directions: (1) in any obvious long direction and (2) perpendicular to the first measurement. The two measurements for each particle were averaged and the aspect ratio for each

---

(7) Vadala, M. L.; Rutnakornpituk, M.; Zalich, M. A.; St. Pierre, T. G.; Riffle, J. S. *Polymer* **2004**, *45*, 7449.

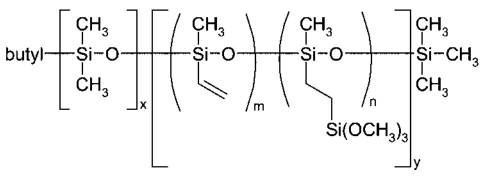

Figure 1. PDMS-*b*-(PMVS-*co*-PMTMS).

particle (longer measurement/shorter measurement) was calculated. The mean and standard deviation were calculated for the particle size and aspect ratio for both fields of view of each sample. Energy-filtered TEM was conducted using the GIF with slit widths of 40 eV at the cobalt $L_{3,2}$ edge (778–793 eV). Pre-edge background images were acquired at 714 and 754 eV, whereas the postedge image was acquired at 799 eV.

X-ray Diffraction. A Siemens D-500 X-ray diffractometer (Cu K_α radiation) was used to acquire X-ray diffraction patterns of the materials before and after heat treatment. Powdered samples were placed onto polycarbonate sample holders and scanned at (1) a rate of 0.2°/min with a step size of 0.03° from 10 to 110° for $\mathbf{N_{1a}}$ and $\mathbf{P_{2a}}$, and (2) a rate of 0.266°/min with a step size of 0.03° from 20 to 100° for $\mathbf{P_{1a}}$.

Magnetic Susceptometry. A Quantum Design magnetic properties measurement system (MPMS-7) equipped with a superconducting quantum interference device (SQUID) sensor was used to make cobalt specific magnetization measurements (σ) at varying applied fields (H) from –70000 to +70000 Oe at 300 and 5 K, with 100 Oe spacings between –1000 and 1000 Oe. Low-temperature measurements were conducted after cooling the sample in both a zero applied field and in an applied field of 70000 Oe. The purpose of the different measurements was to study (1) the saturation magnetization at 300 K, (2) the hysteretic behavior at 300 K, (3) the presence of an exchange bias attributable to a cobalt oxide layer on the surface of the cobalt nanoparticles, and (4) the presence of paramagnetic species due to any residual cobalt carbonyl species in the sample.

Elemental Analysis. Elemental analyses were performed on the materials before and after the heat treatments ($\mathbf{N_{1a}}$, $\mathbf{P_{1a}}$, $\mathbf{P_{2a}}$) using inductively coupled plasma atomic emission spectroscopy (ICP-AES) at the Marine and Freshwater Research Laboratory at Murdoch University, Perth, Western Australia. The samples were prepared by digestion in a 1:1 HNO_3:H_2SO_4 mixture for 14 days at 70–100 °C. The samples and a blank were diluted and analyzed for cobalt concentrations.

X-ray Photoelectron Spectroscopy (XPS). Surface analyses of the cobalt–copolymer nanoparticle assemblies were investigated via XPS before and after the heat treatments. The data was obtained on a Perkin-Elmer X-Ray Photoelectron Spectrometer 5400 series using a Mg anode operating at 300 W (14kV) with the pressure of the system below 5×10^{-6} Pa.

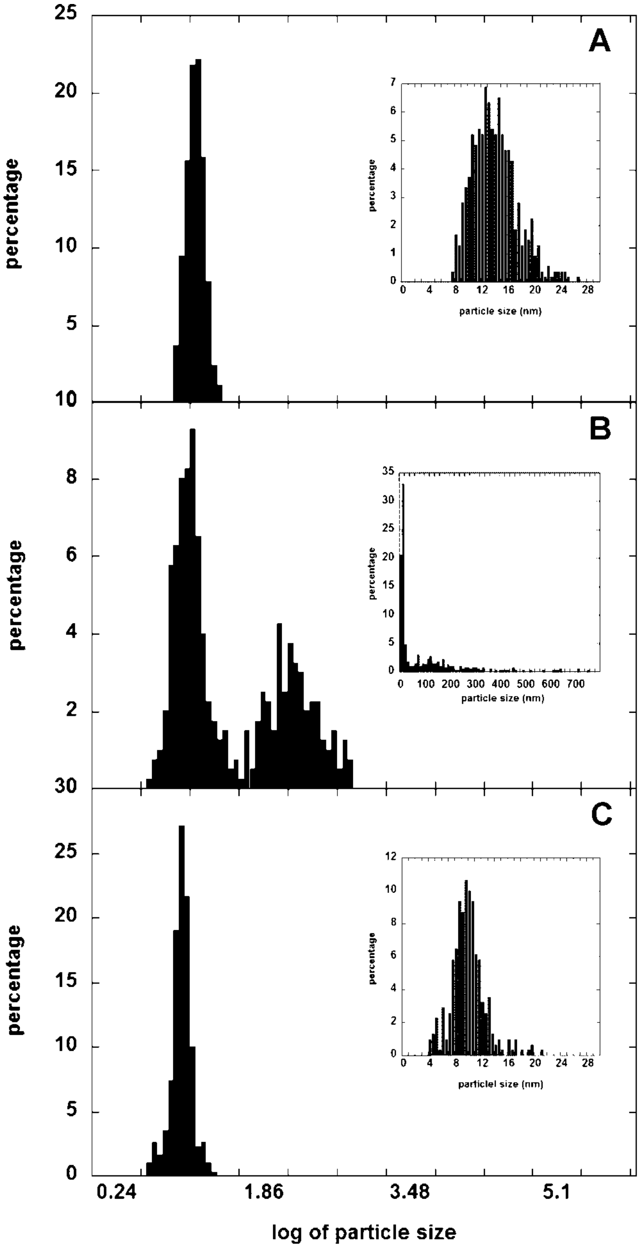

Figure 2. Logged particle size histograms for (A) pre-heat-treated sample ($\mathbf{N_{1a}}$), (B) sample heated at 600 °C ($\mathbf{P_{1a}}$), and (C) sample heated at 700 °C ($\mathbf{P_{2a}}$). Insets show particle size histograms in nanometers. Note: The raw data were logged and rebinned to generate the logged particle size histograms.

Results and Discussion

Transmission Electron Microscopy and X-ray Photoelectron Spectroscopy. TEM was used to study the particle size, size distribution, morphology, chemical composition, and crystallinity of the cobalt–polymer nanoparticle assemblies before and after the elevated temperature steps. The atomic compositions of the surface regions of the nanoparticles were probed by XPS to better understand how the polymer pyrolysis influenced the surfaces. The binding energies of the silicon 1s electrons are centered around 103–104 eV in the XPS spectrum, and this suggests that the many of the silicon species are tri- and tetracoordinated with oxygen. The Si_{1s} peak is broad, however, and this suggests that some silicon species with lower binding energies are also present. Silicons bonded to two oxygens and two carbons typically have binding energies around 102 eV. The oxygen to silicon ratios in the PDMS coated cobalt nanoparticles prior to the heat treatments are consistent with PDMS, as expected. Upon annealing, the carbon content decreases and the O/Si ratio increases substantially. This supports the premise that the surfaces of the annealed nanoparticles have silicons bonded to three and four oxygens.

A "particle" was deemed to be a region with contrast obviously different from the background. The particle size distribution for the material before the heat treatment ($\mathbf{N_{1a}}$) ranged from 8 to 38 nm with a mean of 14.1 nm and mode of 12.5 nm (sample population = 536 particles) (Figure 2A).

The mean aspect ratio was 1.51 with a standard deviation of 0.46. A dramatic difference in particle size and size distribution after thermal treatment at 600 °C ($\mathbf{P_{1a}}$) was apparent. There were two different populations of particles, which resulted in a bimodal particle size distribution (modes at ~10 and 120 nm). The particle size distribution for $\mathbf{P_{1a}}$ ranged from 4 to 750 nm with a mean of 91 nm (sample population = 399 particles) (Figure 2B). The mean aspect ratio for the smaller particles was 1.61 with a standard deviation of 0.5, whereas the mean aspect ratio for the larger particles was 2 with a standard deviation of 0.9. Thermal treatment of $\mathbf{N_1}$ at 700 °C to produce $\mathbf{P_{2a}}$ resulted in a narrow particle size distribution, similar to that of the material that had not been subjected to the high temperature. The particle sizes of $\mathbf{P_{2a}}$ ranged from 4 to 21 nm with a mean of 10.1 nm and a mode of ~9.5 nm (sample population = 310 particles) (Figure 2C). The mean aspect ratio was 1.37 with a standard deviation of 0.34.

It is clear that thermal treatment at 600 °C produces some cobalt nanoparticle growth in addition to the pyrolysis of the polymer. The large particles in the 600 °C heat-treated sample were observed to be polycrystalline. It was reasoned that particle growth occurred before the polymer was completely pyrolyzed to form a protective inorganic shell, and that the large polycrystalline particles observed in the TEM micrographs resulted from sintering of the original cobalt nanoparticles. Jacobsohn et al. reported the increase in size of ion-implanted cobalt nanoparticles in a fused silica matrix after annealing at 900 °C under a vacuum for 10 h.[8] The system reported by Jacobsohn et al. is different from the system discussed here; nevertheless, the particle growth mechanism appears similar. By contrast, it appears that a more rapid pyrolysis of the polymer, such as that which may be achieved at 700 °C, may prevent the cobalt particles from coming into contact with one another and sintering. High-resolution transmission electron micrographs of thin sections of $\mathbf{P_{2a}}$ showed ordered nanoscale coatings surrounding many of the cobalt particles (Figure 3). It may be that this ordered coating prevents cobalt sintering during the heat treatment. Thus, the particles are separated by a siliceous matrix and the average particle size and size distribution remain narrow as in the pre-heat-treated sample. Moreover, the data suggest that the mean particle sizes and size distribution of $\mathbf{P_{2a}}$ (10.07 ± 2.61 nm) may be smaller and narrower than for $\mathbf{N_{1a}}$ (14.14 ± 3.37 nm), although these values are within the standard deviations of the measurements.

Energy filtered TEM (EFTEM) was conducted on $\mathbf{N_{1a}}$, $\mathbf{P_{1a}}$, and $\mathbf{P_{2a}}$ to confirm the elemental identity of the electron dense nanoparticles. As expected, the cobalt distribution maps correlated well with the electron dense regions of the bright-field images (Figure 4).

High-resolution transmission electron microscopy (HRTEM) and X-ray diffraction (described in the next section) were implemented to evaluate the crystallinity of the cobalt nanoparticle complexes with and without the high-temperature heating (annealing) steps. Although $\mathbf{N_{1a}}$ was only weakly crystalline, several high-resolution images were obtained. Figure 5A shows a crystalline particle of $\mathbf{N_{1a}}$ with measured lattice spacings of ~2.01 Å, which are consistent with the {111} plane of fcc cobalt (2.05 Å), but these could also be attributed to the {002} plane of hcp cobalt (2.02 Å).

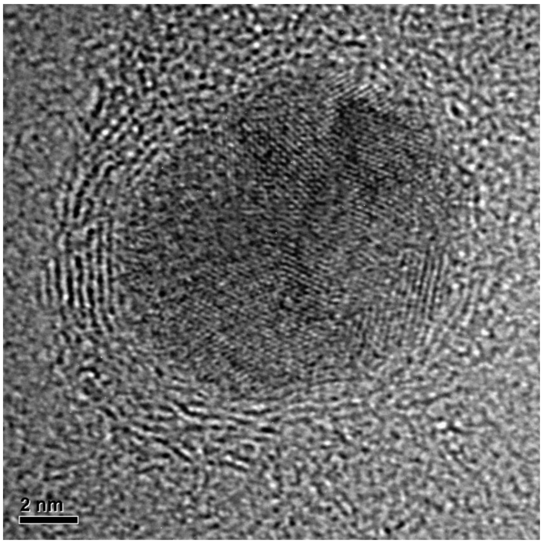

Figure 3. HRTEM of a cobalt nanoparticle (~11 nm in diameter) encased by an ~2 nm thick shell of material exhibiting lattice fringes.

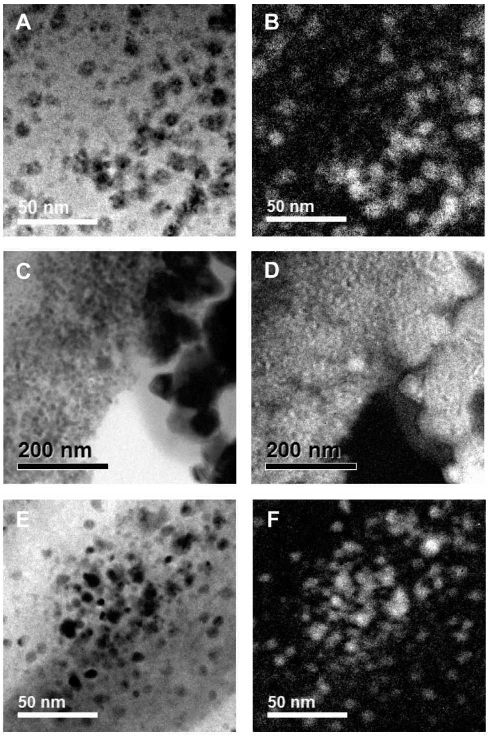

Figure 4. (A) bright field image of $\mathbf{N_{1a}}$, (B) corresponding Co elemental map of A, (C) bright-field image of $\mathbf{P_{1a}}$, (D) corresponding Co elemental map of C, (E) bright-field image of $\mathbf{P_{2a}}$, and (F) corresponding Co elemental map of E.

The X-ray diffraction data show the predominance of fcc cobalt for the materials treated at the elevated temperatures ($\mathbf{P_{1a}}$ and $\mathbf{P_{2a}}$), but the HRTEM images cannot distinguish the dominance of the fcc phase over hcp. A HRTEM image of $\mathbf{P_{1a}}$ also provided evidence of some cobalt in the hcp

---

[8] Jacobsohn, L. G.; Hawley, M. E.; Cooke, D. W.; Hundley, M. F.; Thompson, J. D.; Schulze, R. K.; Nastasi, M. *J. Appl. Phys.* **2004**, *96* (8), 4444.

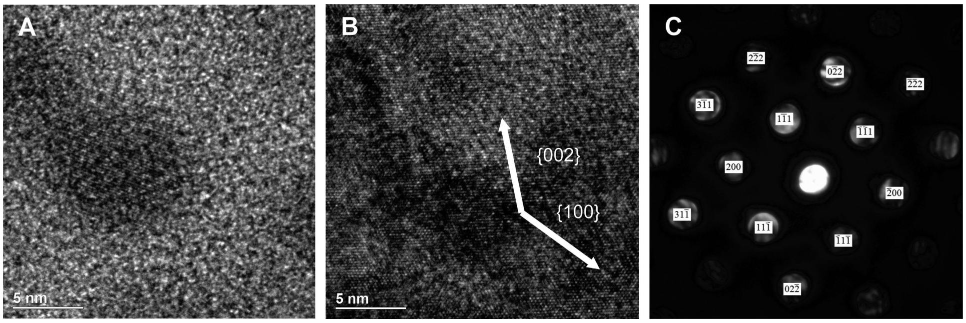

Figure 5. (A) HRTEM image of preheat-treated sample (**N$_{1a}$**), (B) HRTEM image of sample heat-treated at 600 °C (**P$_{1a}$**) showing lattice planes consistent with hcp cobalt structure (arrows normal to denoted lattice planes), and (C) nanobeam electron diffraction of **P$_{1a}$** showing <011> zone axis of fcc cobalt.

Table 2. Comparison of Experimental *d*-Spacing Ratios from SAD Patterns for P$_{1a}$ and P$_{2a}$ with Literature fcc Cobalt *d*-Spacing Ratios[14]

	ratio of lattice planes	experimental	literature
P$_{1a}$	{111}:{200}	1.15	1.15
	{200}:{220}	1.41	1.41
	{220}:{311}	1.19	1.17
	{111}:{220}	1.63	1.63
	{111}:{311}	1.94	1.91
P$_{2a}$	{111}:{200}	1.15	1.15
	{200}:{220}	1.42	1.41
	{220}:{311}	1.17	1.17
	{311}:{222}	1.05	1.04

phase. Figure 5B is a high-resolution image of **P$_{1a}$** with the arrows normal to the {100} and {002} lattice planes of hcp cobalt. Nevertheless, nanobeam electron diffraction (NBD) (Figure 5C) and selected area electron diffraction (SAD) of **P$_{1a}$** provided evidence for the fcc structure of cobalt (Table 2). A high-resolution image of a multitwinned **P$_{2a}$** particle indicated lattice spacings of ~2.04 Å for two twin planes, which is consistent with the {111} of fcc cobalt (2.05 Å) (Figure 6A). Multiple twinning is common in fcc materials[9] and has been reported previously for cobalt nanocrystals.[10] Additional measurements of the Fourier transform of the lower twin in Figure 6A (~1.83 and 1.06 Å) are consistent with the {200} and {311} lattice planes of fcc cobalt (1.77 and 1.07 Å) (Figure 6B). Selected area electron diffraction supports the HRTEM data for **P$_{2a}$**, by also indicating the presence of fcc cobalt (Table 2).

X-ray Diffraction. X-ray diffraction was used to complement electron diffraction, as it provides crystallographic information on macroscopic quantities of sample. X-ray diffraction of the material that had not been heated at the elevated temperatures (**N$_{1a}$**) showed that it was only weakly crystalline, in agreement with the HRTEM data (Figure 7A). Some intense reflections were present at 2θ values of 41.3, 44.7, and 47.4°, corresponding to experimental *d*-spacings of 2.19, 2.03, and 1.92 Å, respectively. These values match well with literature *d*-spacings for hcp cobalt of 2.17, 2.04, and 1.92 Å, respectively; however, the experimental intensities do not follow the same trend as the intensities previously reported in the literature.[11] The energetic difference in atomic stacking between the three known phases of cobalt (fcc, hcp, and epsilon) is low; therefore, having multiple phases of cobalt is possible.[12,13]

From the X-ray diffraction data, it is clear that the dominant phase of the cobalt after being heat treated at 600 °C (**P$_{1a}$**) is fcc. Intense reflections were present at 2θ values of 44.1, 51.5, 75.7, and 92.1°, corresponding to *d*-spacings of 2.05, 1.77, 1.25, and 1.07 Å, respectively. These experimental values match well with the literature values for the {111}, {200}, {220}, and {311} lattice planes of fcc cobalt (Figure 7B).[14] Other less intense peaks were also present, which suggests the minor presence of other phases. The data for **P$_{2a}$** were similar to those of **P$_{1a}$** with major reflections at 2θ values of 44.4, 52, 76, and 92°, corresponding to *d*-spacings of 2.03, 1.76, 1.25, and 1.07 Å, respectively. These reflections, although broader than for **P$_{1a}$**, matched the literature values for fcc cobalt (Figure 7C).[14] Qualitative peak broadening calculations were performed for the materials that had been subjected to heating at 600 (**P$_{1a}$**) and 700 °C (**P$_{2a}$**) using the Scherrer equation. The increased breadth of the **P$_{2a}$** peaks compared with **P$_{1a}$** is consistent with particle size data obtained from TEM, which indicated a smaller mean particle size for **P$_{2a}$**.

Magnetic Susceptometry. Room-temperature σ vs H measurements of the material without high-temperature heat treatment after being exposed to air revealed cobalt specific saturation magnetizations (σ_s) of 48 (aged for 4 months) and 47 emu g^{-1}(aged for 15 months); these values are significantly less than the 161 emu g^{-1} value of bulk cobalt (Figure 8A).[15] The low magnetizations suggest that an oxide layer had formed on both materials. The similarity of these values suggests that the cobalt−copolymer nanoparticles reached the maximum extent of oxidation within 4 months, and the prolonged 15-month exposure did not oxidize the materials further. In addition, **N$_{1a}$** and **N$_{1b}$** did not display any significant magnetic remanence or coercivity. Room-tem-

---

(9) Wang, J.; Tian, M.; Mallouk, T. E.; Chan, M. H. W. *J. Phys. Chem. B* **2004**, *108*, 841.

(10) Murray, C. B.; Sun, S.; Gaschler, W.; Doyle, H.; Betley, T. A.; Kagan, C. R. *IBM J. Res. Dev.* **2001**, *45*, 47.

(11) Hexagonal close-packed (HCP) cobalt, JCPDS card 05–0727. International Centre for Diffraction Data: Newtown Square, PA, 1996; Vol. 22.03.

(12) Dinenga, D. P.; Bawendi, M. G. *Angew. Chem., Int. Ed.* **1999**, *38* (12), 1788.

(13) Puntes, V. F.; Krishnan, K. M.; Alivisatos, A. P. *Science* **2001**, *291*, 2115.

(14) Face-centered cubic (FCC) cobalt, JCPDS card 15–0806. International Centre for Diffraction Data: Newtown Square, PA, 1996; Vol. 44.54.

(15) Bozorth, R. M. *Ferromagnetism*, 5th ed.; D. Van Nostrand Company, Inc.: New York, 1959.

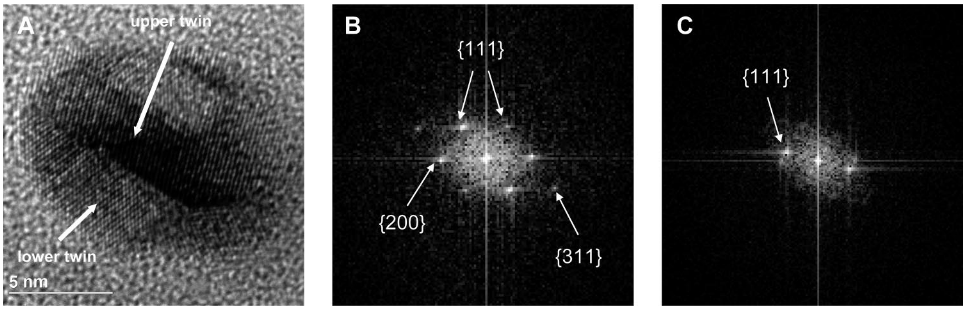

Figure 6. (A) HRTEM image of multitwinned $\mathbf{P_{2a}}$ particle showing lattice planes consistent with fcc cobalt structure, (B) Fourier transform of lower twin in image A, and (C) Fourier transform of upper twin in image A.

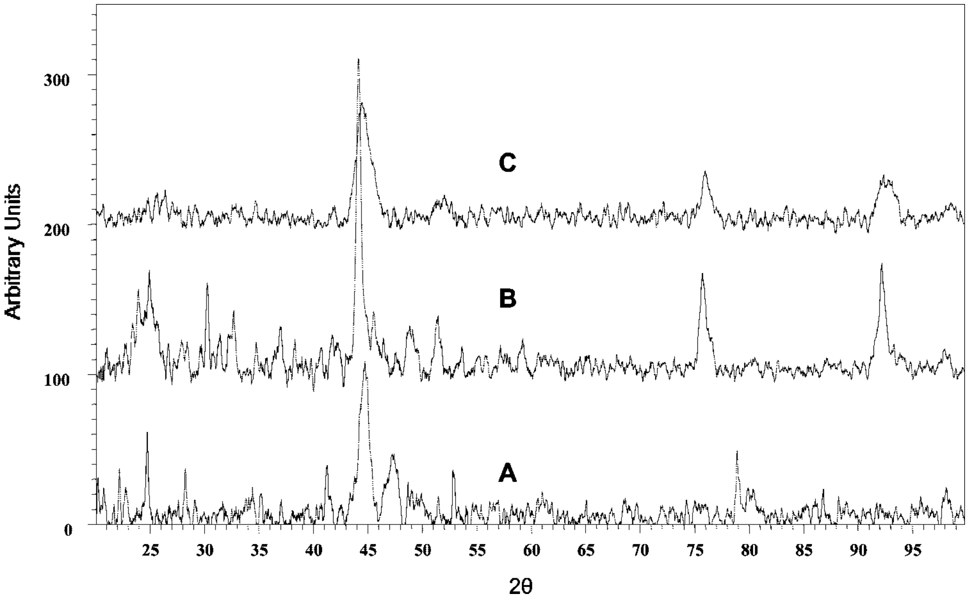

Figure 7. X-ray powder diffraction patterns for (A) $\mathbf{N_{1a}}$, (B) $\mathbf{P_{1a}}$, and (C) $\mathbf{P_{2a}}$.

perature magnetization curves almost saturate in high-applied fields, whereas 5 K magnetization curves have a positive slope in high-applied fields (Figure 8B). The positive slope in the low-temperature magnetization curves suggests the presence of a residual paramagnetic component. The paramagnetic component is believed to be unreacted cobalt carbonyl species that were not incorporated into the cobalt nanocrystals during their synthesis. A slight shift of the field-cooled hysteresis loop with respect to the zero-field-cooled hysteresis loop was observed for $\mathbf{N_{1a}}$ ($H_e \approx 460$ Oe) and is indicative of an exchange bias interaction between an antiferromagnetic cobalt oxide surface layer and a ferromagnetic cobalt metal core (Figure 8B).[16,17] The exchange bias (H_e) for the $\mathbf{N_{1b}}$ material aged for the longer period increased to ~1100 Oe. Because there was no significant decrease in σ_s at room temperature, the increase in H_e suggests a stronger coupling between the cobalt oxide and cobalt. It is possible that the coupling of the cobalt oxide layers with the cobalt particles increased their interfacial order over time and hence strengthened the exchange interaction between the cobalt oxide layer and cobalt core of the nanoparticles. σ vs T measurements indicated that the maximum blocking temperature for the exposed/aged $\mathbf{N_{1a}}$ and $\mathbf{N_{1b}}$ materials was near room temperature.

Cobalt−copolymer nanoparticles were heated at 600 °C for 2 h and then aged in ambient air for 200 days ($\mathbf{P_1}$). This material was not mechanically ground. The cobalt nanoparticles were adequately protected against oxidation, as evidenced by the long-term oxidative stability of the materials. The data indicated that the intact siliceous coating prevented the formation of cobalt oxide on the surfaces of these nanoparticles (Figure 9). σ vs T measurements indicated that the maximum blocking temperature for the $\mathbf{P_1}$ system was near room temperature.

Magnetizations of the materials that had been heated at the elevated temperatures were much higher than those without the heat treatments. Room temperature σ vs H measurements for $\mathbf{P_{1a}}$ indicated a σ_s of 174 emu g^{-1} Co. This is above the reported σ_s for bulk cobalt (161 emu g^{-1}) by 8.75%. This error may be within the reproducibility limits for the elemental analysis measurements. The magnetization curves for $\mathbf{P_{1a}}$ saturate at high-applied fields at room temperature and 5 K (Figure 10A). These data suggest that the heat treatment had eliminated any remaining carbonyl ligands and the paramagnetic cobalt atoms had been incorporated into cobalt nanocrystal lattices.

---

(16) Kiwi, M. *J. Magn. Magn. Mater.* **2001**, *234*, 584.
(17) Nogues, J.; Schuller, I. K. *J. Magn. Magn. Mater.* **1999**, *192*, 203.

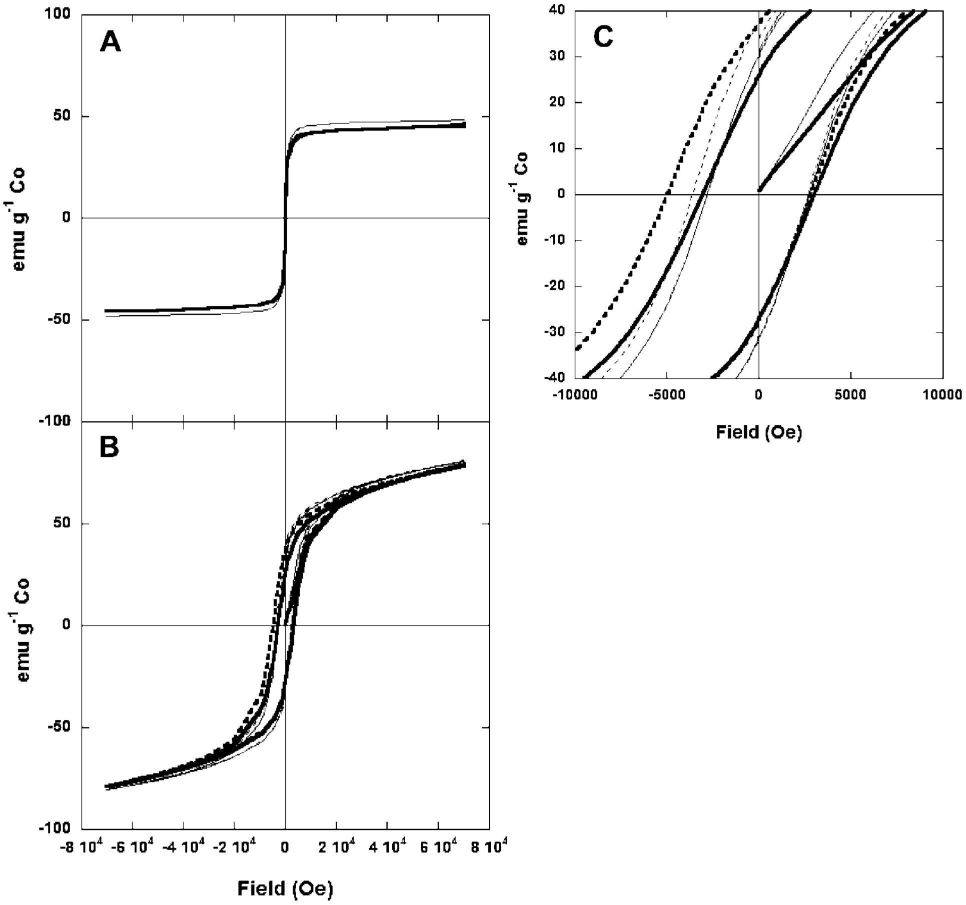

Figure 8. σ vs H measurements conducted on $\mathbf{N_1}$ at (A) 300 K (— $\mathbf{N_{1a}}$; — N_{1b}) and (B) 5 K ($\mathbf{N_{1a}}$, zero-field cooled hysteresis loop —, field cooled hysteresis loop ---; $\mathbf{N_{1b}}$, zero-field cooled hysteresis loop —, field cooled hysteresis loop ---). (C) Enlarged region around the origin for 5 K hysteresis loops showing asymmetric field-cooled hysteresis loop shift.

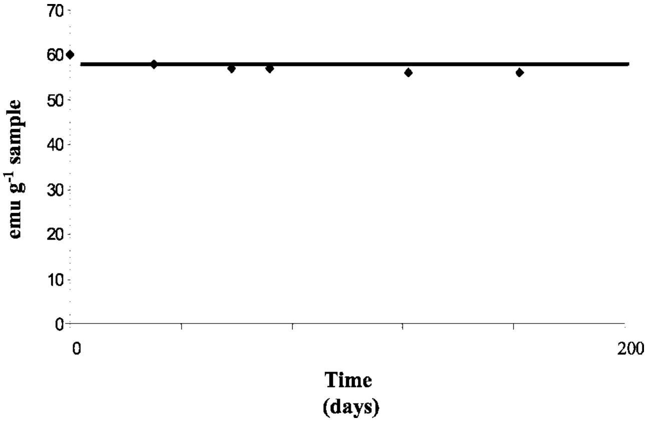

Figure 9. Long-term oxidative stability for unground $\mathbf{P_{1a}}$ was determined by monitoring the saturation magnetization over 200 days.

The oxidative stability of the heat-treated cobalt nanoparticles after being mechanically ground was evaluated over an exposure period of 180 days in ambient conditions. During the 180 days, σ_s for the material that had been heated at 600 °C and ground ($\mathbf{P_{1b}}$) decreased from 174 to 143 emu g^{-1} Co (Figure 11). In addition, the exchange bias field (H_e) increased from 40 to 153 Oe (Figure 11). The decrease in σ_s and increase in H_e over time suggest that cobalt oxide had formed on the surfaces of the cobalt nanoparticles. This implies that mechanically grinding this material may fracture the thin siliceous shells around the nanoparticles, thus exposing bare cobalt. From days 80 to 180, a slight increase in H_e was observed without a decrease in σ_s, and it was reasoned that this might be due to an increase in interfacial order of the antiferromagnetic cobalt oxide layers in contact with the ferromagnetic cores of the cobalt nanoparticles.

Room-temperature σ vs H measurements for $\mathbf{P_{2a}}$ yielded a σ_s of 136 emu g^{-1} Co (Figure 10 A). There is a reasonable decrease in σ_s from $\mathbf{P_{1a}}$ to $\mathbf{P_{2a}}$ (38 emu g^{-1} Co). Although it is unclear why this is so, it may be related to the crystallization process and rate of crystallization of the cobalt nanoparticles. The magnetization curve for $\mathbf{P_{2a}}$ saturates in high-applied fields at room temperature and at 5K (Figure 10 A and B). This is consistent with the hysteresis loops for the material that was heated at 600 °C ($\mathbf{P_{1a}}$). The material that had been heated at 700 °C, mechanically ground, and then aged in air over 180 days ($\mathbf{P_{2b}}$) had a much larger decrease in σ_s from 136 to 31 emu g^{-1} Co, with an increase in H_e from 0 to 156 Oe (Figure 11). One possible cause for the drastic decrease in σ_s for the material heated at 700 vs 600 °C may be related to the much smaller particle size of the cobalt heated at the higher temperature. $\mathbf{P_{2b}}$ comprises cobalt nanoparticles having a small mean particle size of 10.1 nm, whereas $\mathbf{P_{1b}}$ has a bimodal particle size distribution comprising small and large particles, likely attributable to sintering. Thus, $\mathbf{P_{2b}}$ has more surface area than $\mathbf{P_{1b}}$, and more oxidation per unit volume would be expected for $\mathbf{P_{2b}}$.

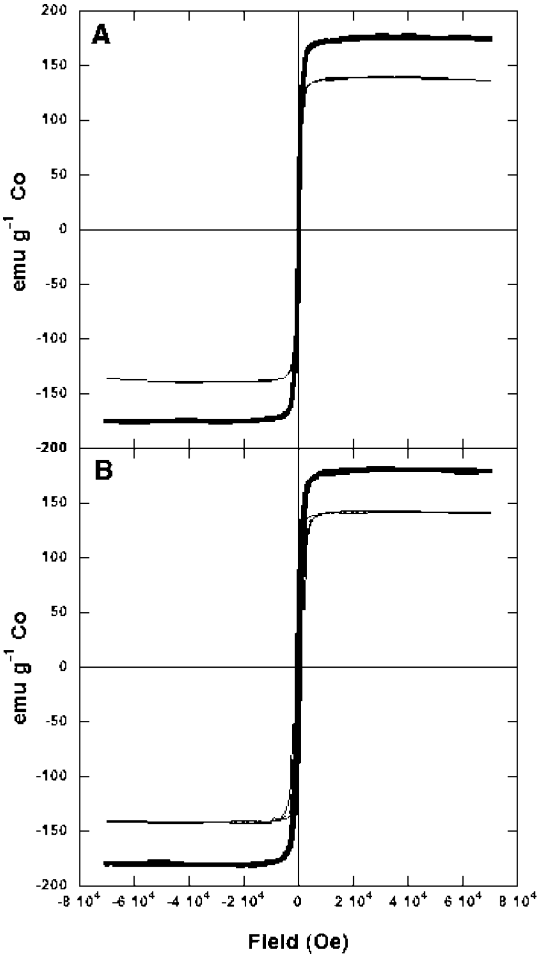

Figure 10. σ vs H measurements conducted on $\mathbf{P_{1a}}$ and $\mathbf{P_{2a}}$ at (A) 300 K (— $\mathbf{P_{1a}}$; — $\mathbf{P_{2a}}$) and (B) 5 K ($\mathbf{P_{1a}}$, zero-field cooled hysteresis loop **—**; field-cooled hysteresis loop **---**; $\mathbf{P_{2a}}$, zero-field cooled hysteresis loop —; field-cooled hysteresis loop ---).

Conclusions

Cobalt nanoparticles were synthesized by thermally decomposing $Co_2(CO)_8$ in poly(dimethylsiloxane-*b*-[methylvinylsiloxane-*co*-methyl-2-trimethoxysilethylsiloxane]) block copolymer solutions. Subsequent heat treatment of the nanoparticles at 600 °C led to an increased particle size distribution, whereas heat treatment at 700 °C afforded a particle size distribution similar to that of the pre-heat-treated material. This may be caused by rapid formation of a siliceous shell around the particles at the higher temperature, which inhibits sintering. σ_s was greater for the heat-treated materials because of an increase in particle crystallinity resulting from annealing of the cobalt nanoparticles. Transmission electron microscopy, electron diffraction, and X-ray diffraction were used to identify the dominant crystal phase of the heat-treated materials as being fcc, although HRTEM analysis indicated the presence of some hcp cobalt. Magnetic susceptometry measurements indicated that the materials without the elevated temperature heat treatments were not stable against oxidation under ambient conditions. The siliceous coatings on the heat-treated materials appear to protect the cobalt surfaces against oxidation, but defects in these coatings are caused by mechanical grinding. These coating defects then lead to exposure of the cobalt nanoparticle surfaces, allowing oxidation to occur.

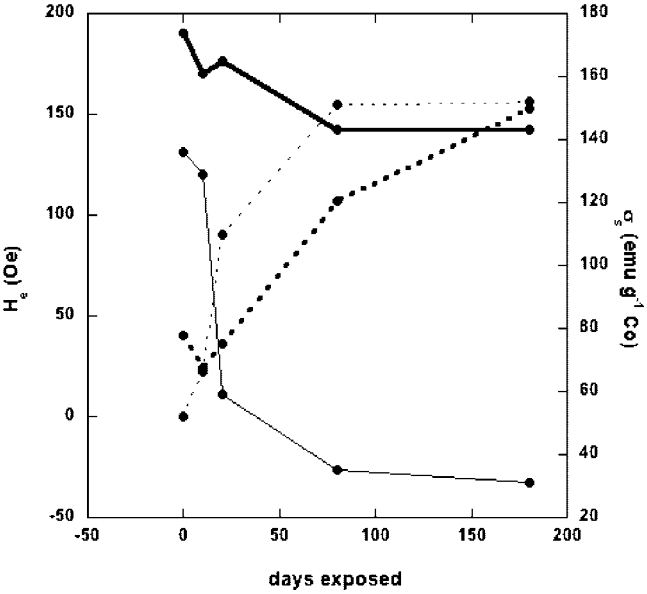

Figure 11. Magnetic susceptometry measurements conducted on $\mathbf{P_{1b}}$ and $\mathbf{P_{2b}}$ while exposing them to air for 180 days indicated that oxidation was taking place as evidenced by a decrease in σ_s and an increase in H_e over time. ($\mathbf{P_{1b}}$ σ_s, **—**; H_e, **---**) ($\mathbf{P_{2b}}$ σ_s, —; H_e, ---).

Future work will focus on creating an oxygen impermeable barrier around discrete, annealed cobalt nanoparticles. In addition, cobalt nanoparticles coated with a siliceous shell provide a means for functionalization of the surfaces of these nanoparticles, which we have already demonstrated and will pursue further.[18]

Acknowledgment. The authors of this paper acknowledge the support of NSF under Contract DMR-0312046, DARPA-AFOSR (Contracts F49620–02–1–0408 and F49620–03–1–0332), OMNOVA Solutions and the Australian Research Council (Grant #DP0559333) for funding. M. A. Zalich thanks the Australian-American Fulbright Commission for a Fulbright Postgraduate Fellowship to conduct research in Australia. The authors would also like to thank John Murphy from the Center for Microscopy and Microanalysis at the University of Western Australia for his assistance with TEM sample preparation.

CM060458L

---

(18) Vadala, M. L.; Zalich, M. A.; Fulks, D. B.; St. Pierre, T. G.; Dailey, J. P.; Riffle, J. S. *J. Magn. Magn. Mater.* **2004**, *92*, 108.